Published in final edited form as:
*Biochemistry*. 2011 May 24; 50(20): 4281–4290. doi:10.1021/bi200341b.

# Probing Domain Interactions in Soluble Guanylate Cyclase†

**Emily R. Derbyshire**[1,#], **Michael B. Winter**[2,‖], **Mohammed Ibrahim**[3,‖,‡], **Sarah Deng**[4], **Thomas G. Spiro**[3], and **Michael A. Marletta**[1,2,5,6,*]
Department of Molecular and Cell Biology, Department of Chemistry, Department of Plant and Microbial Biology, University of California, Berkeley, the Department of Chemistry, University of Washington, Seattle, the California Institute for Quantitative Biosciences, and the Division of Physical Biosciences, University of California, Berkeley, California, 94720-3220

## Abstract

Eukaryotic nitric oxide (NO) signaling involves modulation in cyclic GMP (cGMP) levels through activation of the soluble isoform of guanylate cyclase (sGC). sGC is a heterodimeric hemoprotein that contains a Heme-Nitric oxide and OXygen binding (H-NOX) domain, a Per/ARNT/Sim (PAS) domain, a coiled-coil (CC) domain, and a catalytic domain. To evaluate the role of these domains in regulating the ligand binding properties of the heme cofactor of NO-sensitive sGC, chimeras were constructed by swapping the rat β1 H-NOX domain with the homologous region of H-NOX domain-containing proteins from *Thermoanaerobacter tengcongensis*, *Vibrio cholerae*, and *Caenorhabditis elegans* (*Tt*Tar4H, VCA0720, and Gcy-33, respectively). Characterization of ligand binding by electronic absorption and resonance Raman spectroscopy indicates that the other rat sGC domains influence the bacterial and worm H-NOX domains. Analysis of cGMP production in these proteins reveals that the chimeras containing bacterial H-NOXs exhibit guanylate cyclase activity, but this activity is not influenced by gaseous ligand binding to the heme cofactor. The rat-worm chimera containing the atypical sGC Gcy-33 H-NOX domain was weakly activated by NO, CO and $O_2$, suggesting that atypical guanylate cyclases and NO-sensitive guanylate cyclases have a common molecular mechanism for enzyme activation. To probe the influence of the other sGC domains on the mammalian sGC heme environment, heme pocket mutants (Pro118Ala and Ile145Tyr) were generated in the β1 H-NOX construct (residues 1–194), the β1 H-NOX-PAS-CC construct (residues 1–385), and the full-length α1β1 sGC heterodimer (β1 residues 1–619). Spectroscopic characterization of these proteins shows that inter-domain communication modulates the coordination state of the heme-NO complex and the heme oxidation rate. Taken together, these findings have important implications for the allosteric mechanism of regulation within H-NOX containing proteins.

†Funding was provided by NIH grant GM077365 to M.A.M.

*To whom correspondence should be addressed at University of California, Berkeley, QB3 Institute, 570 Stanley Hall, Berkeley, CA 94720-3220. Phone: (510) 666-2763; Fax: (510) 666-2765;, marletta@berkeley.edu.
‖M.B.W. and M.I. contributed equally to this paper.
#Present address: Harvard Medical School, Department of Biological Chemistry and Molecular Pharmacology, Boston, MA 02115.
‡Present address: Thermo Fisher Scientific, 355 River Oaks Parkway, San Jose, CA 95134.
[1]Department of Molecular and Cell Biology, University of California, Berkeley
[2]Department of Chemistry, University of California, Berkeley
[3]Department of Chemistry, University of Washington, Seattle
[4]Department of Plant and Microbial Biology, University of California, Berkeley
[5]California Institute for Quantitative Biosciences
[6]Division of Physical Biosciences, Lawrence Berkeley National Laboratory

Supporting Information. Spectra of sGC mutants (Figure S1), activity of sGC α1β1 P118A (Figure S2), NO dissociation time courses from β1 I145Y mutants (Figure S3, Table S1), and resonance Raman spectra of β1(1–194) mutants in the $Fe^{II}$-unligated state (Figure S4). This material is available free of charge via the Internet at http://pubs.acs.org.

Soluble guanylate cyclases (sGCs) are heterodimeric hemoproteins that respond to gaseous signaling molecules. The best-characterized eukaryotic sGCs contain a heme cofactor that rapidly binds nitric oxide (NO), but does not bind oxygen ($O_2$). Additionally, the heme iron is stable in the ferrous oxidation state. This selective binding of NO enables the protein to function as an essential NO sensor in mammals. Worms and flies are known to contain atypical sGCs that are distinct from mammalian sGC as they bind and respond to $O_2$ in addition to NO and carbon monoxide (CO). Despite these differences in ligand selectivity, both non-$O_2$ binding and $O_2$ binding sGCs perform critical physiological roles by synthesizing cyclic GMP (cGMP) (1–4).

The best-characterized non-$O_2$ binding sGC heterodimer is the rat α1β1 protein. The α1 and β1 subunits are highly homologous, and both proteins consist of four distinct domains (reviewed in (5)). The β1 subunit, which is the heme-binding subunit, contains an N-terminal Heme-Nitric oxide and OXygen (H-NOX) binding domain, a Per/ARNT/Sim (PAS) domain, a coiled-coil (CC) domain and a C-terminal catalytic domain (Figure 1A). Predicted $O_2$-binding sGCs from Drosophila and *C. elegans* also contain H-NOX, PAS, CC and catalytic domains based on primary sequence analysis.

Previously characterized heme binding truncations of the β1 subunit include the H-NOX construct β1(1–194) (6) and the H-NOX-PAS-CC construct β1(1–385) (7). Several bacterial H-NOX proteins with homology to β1(1–194) have been characterized. These homologs are not fused to guanylate cyclase domains, but are thought to be involved in gaseous signaling. Some H-NOX homologs are fused to predicted methyl-accepting chemotaxis proteins, like the $O_2$-binding H-NOX domain from *Thermoanaerobacter tengcongensis*, while others are associated with histidine kinases, like the H-NOX protein from *Vibrio Cholerae*, or diguanylate cyclases. To date, there is no crystal structure of an H- NOX domain from a guanylate cyclase; however, the structures of three bacterial H-NOX proteins with high homology to β1(1–194) have been determined (8–11). These structures have guided many proposals on sGC activation and regulation, yet the precise function of each domain in the mammalian enzyme remains to be determined. Additionally, the functional and structural homology between the bacterial H-NOX proteins, the eukaryotic $O_2$-binding H-NOX proteins, and the eukaryotic non-$O_2$ binding H-NOX proteins is unknown. To address these questions, chimeric proteins were constructed by replacing the rat β1 H-NOX domain with bacterial or eukaryotic H-NOX domains. We found that enzyme sensitivity to gaseous ligand binding (NO, $O_2$ and CO) is observed when the β1 H-NOX is replaced with an atypical guanylate cyclase H-NOX domain from *Caenorhabditis elegans* (Gcy-33), but this sensitivity is abolished by replacement of the sGC heme domain with two of its bacterial homologs (*Tt*Tar4H H-NOX and VCA0720 H-NOX). This suggests that NO-sensitive and atypical guanylate cyclases have a common mechanism of communication between the H-NOX domain and catalytic domains and/or contain domains that exhibit a relatively high degree of structural homology. To further probe the role of the PAS, CC and catalytic domains in modulating the ligand binding properties of sGC, two residues (Tyr145 and Pro118, Figure 1) known to be important for $O_2$ binding and/or heme conformation in *Tt* H-NOX (12, 13) were mutated in the full-length α1β1 heterodimer, β1(1–385), and β1(1–194). Our results with these mutants highlight the allosteric influence that the α1 subunit and the β1 PAS, CC and catalytic domains have over the heme environment.

## MATERIALS AND METHODS

### Reagents

Primers were obtained from Elim Biopharmaceuticals. Sf9 cells were obtained from the Department of Molecular and Cell Biology Tissue Culture Facility, University of California,

Berkeley. Diethylammonium (*Z*)-1-(*N*,*N*-diethylamino)diazen-1-ium-1,2-diolate (DEA/NO) was from Cayman Chemical Co.

### Generation of sGC chimeras, protein expression, and purification

Alignments of various H-NOX domains were done with MegAlign (LaserGene, DNAStar Inc.) to guide chimera construction. The N- terminal residues of *Tt*Tar4H (1–180), VCA0720 (1–178), and Gcy-33 (1–184) were fused to rat β1 residues 187–619 for *Tt*_β1 and Gcy33_β1 or residues 181–619 for *Vc*_β1, and then cloned into pFastBac (Invitrogen). All constructs were verified by sequencing (University of California, Berkeley DNA Sequencing Facility). For the chimera expression the Bac-to-Bac baculovirus expression system (Invitrogen) was used to generate recombinant baculovirus according to the manufacturer's instructions. Sf9 cells were coinfected with wild-type α1 and chimeric β1 constructs. α1/*Tt*_β1, α1/*Vc*_β1 and α1/Gcy33_β1 were purified using a previously reported procedure (14) with a few modifications. After elution from the Ni affinity resin, α1/*Tt*_β1 was exchanged into a 0 mM NaCl buffer and then applied to an anion-exchange column. After washing, the column was developed with a gradient of 0–150 mM NaCl in elution buffer. α1/*Vc*_β1 purified with a substoichiometric amount of heme and was reconstituted. To reconstitute the protein, 1.5–2 equivalents of hemin were added to the protein and the sample was left on ice for 12 hrs to allow the reaction to equilibrate. Excess hemin was then removed by applying the protein to a PD-10 column equilibrated with 50 mM Hepes, pH 7.4, 50 mM NaCl, 5 mM dithiothreitol (DTT). The protein was characterized both as isolated and after heme reconstitution to ensure the procedure did not affect heme ligand binding.

### Generation of mutants, protein expression, and purification

Mutants of rat β1 (P118A and I145Y) were generated using the QuikChange XL site-directed mutagenesis kit (Stratagene) according to the manufacturer's instructions. The accuracy of each substitution was verified by sequencing (University of California, Berkeley DNA Sequencing Facility).

Rat β1(1–194) and β1(1–385) were expressed and purified by a method that was slightly modified from an existing protocol (6). Specifically, constructs were transformed into *E. coli* Tuner(DE3) competent cells. Expression cultures for β1(1–194) and β1(1–385) were grown at 37 °C to an $Abs_{600}$ of 0.6 - 0.7 and were then cooled to 20 °C. Protein expression was induced by the addition of IPTG to a final concentration of 0.5 mM and cultures were supplemented with aminolevulinic acid to a final concentration of 0.1 mM for all constructs except β1(1–385) P118A which was induced with 1 mM IPTG in the absence of aminolevulinic acid. Cells were harvested by centrifugation 15–18 h post- induction, and cell pellets were stored at −80 °C. Frozen cell pellets from 2 or 3 L of culture were thawed and resuspended in 50 mL of buffer A [50 mM DEA, pH 8.5, 20 mM NaCl, 5 mM DTT, 1 mM Pefabloc (Pentapharm), and 5% glycerol]. Resuspended cells were lysed with an Emulsiflex-C5 high-pressure homogenizer and centrifuged for 90 min at 100000 *g*. The supernatant was applied to a Toyopearl SuperQ 650 M (Tosohaas) anion-exchange column and a gradient was developed from 20 to 500 mM NaCl. Fractions containing the protein of interest were concentrated and then applied to a prepacked Superdex S75 HiLoad 16/60 gel-filtration column (Pharmacia) for β1(1–194) or a prepacked Superdex S200 HiLoad 16/60 gel-filtration column (Pharmacia) for β1(1–385). The gel filtration buffer was 50 mM TEA, pH 7.5, 150 mM NaCl, 5 mM DTT, and 5% glycerol. Protein was then pooled, concentrated, and stored at −80 °C. Protein concentrations were determined using the Bradford Microassay (Bio-Rad Laboratories). β1(1–385) P118A, β1(1–385) P118A/I145Y and β1(1–194) P118A were isolated with a substoichiometric amount of heme and were reconstituted using the method described above for the α1/*Vc*_β1 heme reconstitution. These proteins

were characterized both as isolated and after heme reconstitution to ensure the procedure did not affect heme ligand binding.

The Bac-to-Bac baculovirus expression system (Invitrogen) was used to generate recombinant baculovirus according to the manufacturer's protocol for the expression of β1 P118A. Sf9 cells were cultured and recombinant α1β1 P118A was purified according to a previously published protocol (14) with the following modification. sGC collected from the Ni affinity resin was treated with 1.5 equivalents of hemin in 25 mM TEA, pH 7.5, 50 mM NaCl, 5 mM DTT, and placed on ice for 12 hrs. After this procedure the protein was applied to an anion-exchange column as reported for the purification of wild-type α1β1 (15). Protein purity was assessed by SDS-PAGE (purity > 95%) and concentrations were determined using the Bradford Microassay (Bio-Rad Laboratories). The protein was characterized both as isolated and after heme reconstitution to ensure the procedure did not affect enzyme activity or ligand binding.

## Enzyme assays

Duplicate end-point assays were performed for sGC chimeras at 25 °C and for α1β1 P118A at 37 °C as previously described (16). Briefly, sGC complexes were formed with DEA/NO (100 μM) or CO gas (Praxair, Inc.) and confirmed with electronic absorption spectroscopy. Assay mixtures for α1β1 P118A contained 0.2 μg of protein, 50 mM Hepes, pH 7.4, 1 mM DTT, 3 mM $MgCl_2$, 1.5 mM GTP and 150 μM YC-1 (in DMSO) where indicated. Assay mixtures for chimeras contained 0.2 - 1 μg of protein, 50 mM Hepes, pH 7.4, 50 mM NaCl, 1 mM DTT, 4 mM $MgCl_2$, 2 mM GTP and 150 μM YC-1 (in DMSO) where indicated. Chimera assays of $Fe^{II}$ or $Fe^{II}$-CO complexes were done in the presence of 100 μM sodium dithionite and limited $O_2$. All assays were in a final volume of 100 μL and contained 2% DMSO, which was shown not to affect enzyme activity. Reactions were quenched after 2 minutes for α1β1 P118A or 5 minutes for sGC chimeras by the addition of 400 μL of 125 mM $Zn(CH_3CO_2)_2$ and 500 μL of 125 mM $Na_2CO_3$. cGMP quantification was carried out using a cGMP enzyme immunoassay kit, Format B (Biomol), per the manufacturer's instructions. Each experiment was repeated 3 times to ensure reproducibility.

## Kinetics

The oxidation rates of β1(1–385) P118A and β1(1–194) P118A were determined using a stopped-flow spectrophotometer (TgK Scientific) at 10 °C and 37 °C, respectively. Samples of anaerobic $Fe^{II}$ protein were combined with an equal volume of air-saturated (21% $O_2$) buffer (50 mM Hepes, pH 7.4, 50 mM NaCl). For β1(1–385) P118A, a small amount of sodium dithionite (2 equivalents) was present during mixing which was found to be necessary to keep the protein fully reduced during subsequent manipulations. The observed $O_2$-binding rate and oxidation rate of β1(1- 385) P118A/I145Y was measured using electronic absorption spectroscopy at 37 °C. Spectra were collected after addition of 150 μL of $O_2$ saturated buffer to the $Fe^{II}$ protein in 150 μL of anaerobic buffer. The change in the absorbance maximum versus time was plotted and the data were fit to a single exponential equation. Dissociation of NO from the heme of sGC was measured at 25 °C using the CO/dithionite trapping method described previously (17). The change in the absorbance maximum versus time was plotted and the data were fit to a double exponential equation. The time courses shown are representative results of experiments repeated 2–6 times for each construct.

## Resonance Raman spectroscopy

RR spectra were collected for samples in spinning NMR tubes via backscattering geometry at room temperature. The protein (~10 μM heme) was in 50 mM Hepes, pH 7.4, 50 mM NaCl, 1 mM DTT and 150 μM YC-1, where indicated. The excitation wavelengths at 430

nm (for ligand-free samples) and 413 nm (for CO-bound samples) were obtained by frequency doubling, using a nonlinear lithium triborate crystal, of a Ti:sapphire laser (Photonics International TU-UV), which was pumped by the second harmonic of a Q-switched Nd:YLF laser (Photonics Industries International, GM-30-527). For CO-bound samples, laser power at the sample was kept to a minimum (less than 1 mW) by using a cylindrical lens to avoid the photolysis of bound CO. For ligand-free samples, laser power at the sample was 2–3 mW. Scattered light was collected and focused onto a single spectrograph (SPEX 1269) equipped with a CCD detector (Roper Scientific) operating at −110 °C. Spectra were calibrated with dimethyl formamide and DMSO-$d_6$. A Grams A/I software (Thermo- Galactic) was used to analyze the spectra.

## RESULTS & DISCUSSION

sGC is a heterodimeric hemoprotein where each protein subunit consists of four distinct domains (Figure 1A). Proteins with homology to each of the four domains have been elucidated by X-ray crystallography, but there is no structure of the full-length, multi-domain protein. In the work reported here, sGC chimeras were designed and characterized to evaluate the structural and functional similarity between sGC and prokaryotic and eukaryotic homologs of sGC and to illuminate aspects of inter-domain communication in lieu of a full-length sGC structure.

### Characterization of sGC chimeras

Previous studies have shown that the β1 PAS, CC and catalytic domains are essential to protein dimerization, while the N-terminal H-NOX domain is essential to gaseous ligand sensing (reviewed in (18)). When NO binds to the rat sGC H-NOX domain, cGMP synthesis increases several hundred-fold. To determine if guanylate cyclase activity can be regulated by β1 H-NOX homologs, the β1 H-NOX domain in the rat sGC was replaced with bacterial and worm H-NOX domains. Specifically, three different H-NOX proteins were fused to the β1 PAS-CC-C domain (Figure 1B); *Tt*Tar4H H-NOX, *V. cholerae* VCA0720 H-NOX, and *C. elegans* Gcy-33 H-NOX (*Tt*_β1, *Vc*_β1, and Gcy33_β1). The β1 sequence was replaced with *Tt* H-NOX, *Vc* H-NOX and Gcy-33 H- NOX sequences with 17, 25 and 27% identity, respectively (determined with Lasergene, DNAStar, Inc.). *Tt* H-NOX has the advantage of being an $O_2$-binding H-NOX whose structure has been solved, while *V. cholerae* is a non-$O_2$ binding prokaryotic H-NOX with greater sequence homology to the β1 H- NOX domain, although no structure has yet been determined. The heme domain from Gcy-33 has not been biochemically characterized, but it is known to be an atypical guanylate cyclase (reviewed in (19)) that mediates an $O_2$-dependent behavior in worms (20). This observation, in addition to the presence of a tyrosine at position 145 (rat β1 numbering), strongly suggests the protein binds $O_2$ (21).

The fusion proteins were cloned and then co-expressed with the rat α1 subunit in a Sf9/baculovirus system. The resulting chimeric heterodimer was purified using Ni-NTA metal affinity chromatography, where the tag is on the α1 protein, followed by anion exchange chromatography. All constructs purified as heterodimers and were greater than 95% pure based on SDS-PAGE. Both prokaryotic chimeras were expressed and purified with yields that were 2–3-fold greater than rat α1β1, suggesting that domain swapping might be a useful method to increase protein yields. The α1/*Tt*_β1 heterodimer as isolated had an electronic absorption maximum between 418–420 nm (Table 1). This species is likely the $Fe^{II}$- $O_2$ complex based on its similarity to other $O_2$-bound heme proteins (22, 23). After reduction with sodium dithionite, the ferrous-unligated protein was found to form 6-coordinate complexes with $O_2$, CO and NO (Figure 2, Table 1). The ability to bind $O_2$ and the formation of a 6-coordinate $Fe^{II}$-NO complex demonstrates that the α1/*Tt*_β1 chimera has properties more like the bacterial *Tt* H-NOX protein (23) than mammalian β1 H-NOX (6).

The α1/*Vc*_β1 heterodimer was isolated as a mixture of apo and heme-bound protein. After reconstitution with heme, the protein formed a 6-coordinate complex with CO and a 5-coordinate complex with NO, similar to the wild-type *Vc* and β1 H-NOXs (6, 23). α1/Gcy33_β1 was isolated heme-bound and required reduction with sodium dithionite to form a reduced $Fe^{II}$–unligated species. After reduction, the Soret maximum shifted in the presence of NO, CO and $O_2$ to 422, 421, and 418 nm, respectively (Figure 2). Biochemical characterization of full-length Gcy-33 has not been reported so these results cannot be compared to the wild-type protein; however, the deviations of these Soret values from wild-type α1β1 suggests that the *C. elegans* atypical cyclase forms 6-coordinate complexes with NO, CO and $O_2$. This indicates that Gcy-33 has biochemical properties similar to the related Drosophila atypical guanylate cyclase, Gyc-88E (24) and supports *in vivo* data that suggests the protein functions as an $O_2$ sensor in worms (20).

To determine if the mammalian H-NOX domain homologs can regulate guanylate cyclase activity, cGMP synthesis was measured in the presence of various heme ligands. The α1 and β1 catalytic domains formed a functional dimer since each chimera exhibited a basal activity (Table 2). Interestingly, α1/Gcy33_β1 exhibited a basal activity that was significantly greater than the α1β1 basal activity (326 nmol $min^{-1}$ $mg^{-1}$ versus 50–100 nmol $min^{-1}$ $mg^{-1}$ for α1β1). The atypical cyclase Gyc-88E homodimer also exhibited a relatively high basal activity when compared to α1β1 (24). While all of the chimeras exhibited a basal activity, NO did not activate α1/*Tt*_β1 and α1/*Vc*_β1. Additionally α1/*Tt*_β1 was not activated by CO or $O_2$ and YC-1 did not activate the protein in the unligated, $Fe^{II}$-CO or $Fe^{II}$-NO bound states (Table 2). YC-1 is a small molecule that synergistically activates sGC in the presence of CO and NO (25). Thus, replacement of the β1 H-NOX domain with either the *T. tengcongensis* or *V. cholerae* bacterial H-NOXs abolished the sensitivity of these chimeric sGCs to NO. However, cGMP synthesis of α1/Gcy33_β1 increased 1.5-2-fold in the presence of NO, CO and $O_2$ (Figure 3). Therefore, this atypical guanylate cyclase H-NOX domain maintains some β1-like function when fused to the β1 PAS, CC and catalytic domain.

The absence of enzyme sensitivity to NO, CO and $O_2$ in the rat-bacterial chimeras suggests that ligand binding to these proteins does not induce the same conformational change as is observed with the α1β1 heterodimer. Several factors could contribute to this loss of sensitivity; the communication between the heme binding pocket and the catalytic domains may be disrupted, the prokaryotic H-NOXs could utilize a different allosteric mechanism of domain regulation, or the prokaryotic H-NOX domains could undergo a conformational change upon NO binding that is distinct from that of the β1 H-NOX domain. To further address these possibilities, resonance Raman (RR) spectroscopy was used to evaluate how the mammalian sGC PAS, CC, and catalytic domains influence the H-NOX heme environment in the context of the chimeric proteins.

RR spectroscopy has been previously used to examine the heme environment of *Tt* H-NOX, *Vc* H-NOX and rat α1β1 (23, 26). The RR spectra of α1/*Tt*_β1 and α1/*Vc*_β1 were collected for this work and compared to the previously published reports. RR spectra of the Gcy 33 construct could not be obtained due to high background fluorescence of the sample. The $Fe^{II}$-CO spectrum of α1/*Tt*_β1 shows that the FeC and CO frequencies are observed as single bands at 489 $cm^{-1}$ and 1987 $cm^{-1}$, respectively (Figure 4, Table 3). These values are similar to those reported for the *Tt* H-NOX $Fe^{II}$-CO complex (490 and 1989 $cm^{-1}$, respectively) (23). Additionally, the heme skeletal markers in the high-frequency region and the porphyrin conformation-sensitive bands in the low-frequency region are similar to those observed with wild-type *Tt* H-NOX. The RR spectrum did not change upon addition of YC-1, indicating that the small molecule does not bind to this protein or YC-1 is no longer able to induce a conformational change within the heme pocket when it binds. This result is

in agreement with the activity studies (vide infra), which showed that YC-1 did not activate the protein.

The $Fe^{II}$-CO RR spectrum of α1/*Vc*_β1 shows that the νFeC frequency is observed at 489 $cm^{-1}$ (Figure 4), which is similar to the value reported for wild-type *Vc* H-NOX (491 $cm^{-1}$) (23). The weak νCO mode was not observed due to the high fluorescence background of the sample; however, based on the ν FeC frequencies of both α1/*Tt*_β1 and α1/*Vc*_β1 it seems that the anomalously low backbonding in α1β1 (26) cannot be induced in the prokaryotic H-NOX domains with fusion to the β1 subunit. Interestingly, some heme skeletal marker bands in the high-frequency region shifted from the *Vc* H- NOX values such that they are closer to the values for α1β1 (Table 3). Specifically, $\nu_2$, $\nu_3$ and $\nu_4$ upshift by 4, 11 and 3 $cm^{-1}$, respectively, and this shows that the *Vc* H-NOX heme environment is indeed influenced by the presence of the PAS, CC and catalytic domains. YC-1 addition produces no spectral change, except for a broadening of the $\nu_{FeC}$ band, possibly signaling a minor species with an altered FeCO conformation.

YC-1 is thought to bind to the N-terminus of the α1 subunit (27–29) and this binding event is known to affect the sGC heme conformation (30, 31). Some communication between this binding site and the heme pocket also occurs in the α1/*Vc*_β1 chimera, but this communication is not sufficient to induce activity changes as evidenced by the lack of YC-1-induced activation (Table 2). Together these RR results suggest that the non $O_2$-binding prokaryotic H-NOX shares a more homologous structure to the rat β1 H-NOX domain than the $O_2$-binding prokaryotic H-NOX. This would enable the *Vc* H-NOX domain to respond to the β1 PAS, CC and catalytic domains and undergo a modest conformational change upon YC-1 binding.

The observation that the *Tt* H-NOX domain was apparently unaffected by fusion to the β1 protein, shows that some H-NOX proteins do not have the ability to retain even partial function with domain swapping. Perhaps the mechanism of regulation between $O_2$-binding and non $O_2$-binding prokaryotic H-NOXs is too divergent to allow for the retention of function. Conversely, when fused to the β1 protein the predicted $O_2$-binding eukaryotic H-NOX domain from a guanylate cyclase was responsive to the presence of NO, $O_2$ and CO. This argues for some commonality in the mechanism of activation in $O_2$-binding and non $O_2$-binding guanylate cyclases, but the varying degree of ligand induced activation in α1β1 and α1/Gcy33_ β1 highlights the mechanistic and/or structural differences between these two classes of sGCs.

## Critical heme pocket residues

In order to further probe the influence of the sGC PAS, CC, and catalytic domains on H-NOX ligand binding properties and heme environment, site-directed mutagenesis experiments were carried out on mammalian sGC domain truncations – β1(1–194) and β1(1–385) – and full-length protein. The β1(1–194) construct contains the H-NOX domain alone, and the β1(1–385) construct contains the H-NOX, PAS, and CC domains (Figure 1B). Two residues in the sGC heme pocket were chosen for site-directed mutagenesis experiments aimed at probing the involvement of the PAS, CC and catalytic domains in heme ligand binding. Investigations with the $O_2$- binding H-NOX domain from *T. tengcongensis* have revealed a proximal pocket proline (Pro118 in the rat β1 numbering system) that is important for maintaining the heme conformation (12, 13) (Figure 1C). In addition to affecting the protein heme conformation, mutation of proline 118 to alanine in *Tt* H-NOX increases $O_2$ affinity (12) and increases the proximal Fe-His bond strength (13). Residue 145 (in the rat β1 numbering system) is another critical residue in H-NOX proteins (Figure 1C). Generally, in $O_2$-binding H-NOX proteins, position 145 is a tyrosine, while an isoleucine or leucine is most commonly present in non $O_2$-binding H-NOX proteins like β1.

A kinetic study showed that Tyr145 is critical for $O_2$ binding in *Tt* H-NOX (32). To probe the function of this distal pocket residue in β1, Ile145 was replaced with a tyrosine in β1(1–385) (I145Y). This mutation produced a protein that was capable of binding $O_2$ (32); however, further studies showed that the same mutation in the full-length α1β1 heterodimer did not produce an $O_2$-binding protein (33, 34). In this work, a comparative study with different sGC β1 chain lengths (Figure 1A) was carried out with modification of the conserved heme pocket residues 118 and 145.

## Ligand binding to β1 P118A and β1 I145Y mutants in full-length α1β1 and H-NOX domain constructs

Ligand binding and $O_2$ reactivity in Pro118 and Ile145 mutants of α1β1, β1(1–385) and β1(1–194) were examined. The electronic absorption maxima for the $Fe^{II}$, $Fe^{II}$-NO and $Fe^{II}$-CO complexes in α1β1 and H-NOX domain mutants are reported in Table 4. Unlike the *Tt* H-NOX P118A mutant, all β1 P118A mutants were isolated with a substoichiometric amount of heme, determined by the ratio of the Soret maximum (428 nm) to the total protein absorbance (280 nm) compared to that of the wild-type protein. Pro118 would appear to be important for heme affinity in sGC α1β1, but not as critical for that in *Tt* H- NOX. Mutants isolated with a substoichiometric amount of heme were successfully reconstituted. All mutants were then reduced with sodium dithionite and these reduced proteins exhibited absorbance maxima between 424–431 nm (Figure S1). After exposure to CO, the absorbance maxima shifted to 420–423 nm, indicative that all formed a 6-coordinate $Fe^{II}$-CO complex. Both α1β1 P118A and β1(1- 194) P118A form a stable 5-coordinate complex with NO after displacement of the proximal histidine residue, while β1(1–385) P118A oxidizes rapidly in the presence of either NO or $O_2$. Characterization of β1 P118A mutants before and after reconstitution confirms that this procedure did not affect the ligand binding properties of the protein.

Enzyme assays were performed to test if alteration of the conserved Pro118 residue affects sGC activity. The mutant had a basal activity that was similar to that of the wild-type protein (Figure S2). This activity increased 40–50-fold in the presence of NO and 1–2-fold upon CO binding. A similar fold-increase was observed with the protein that was not reconstituted with heme, suggesting that the procedure did not affect catalysis. Thus, sGC α1β1 P118A exhibits a reduction in maximal NO, CO and YC-1-stimulated activity when compared to wild-type sGC. A reduction in maximal enzyme activation was also observed when conserved distal pocket residues were mutated in sGC α1β1 (17), so, not surprisingly, both distal heme pocket and the proximal heme pocket (Pro118) residues are important for enzyme activation.

In agreement with a previous report, a $Fe^{II}$-$O_2$ complex was observed in β1(1–385) after the introduction of a tyrosine at position 145 (32); however, the same mutation in either the full-length α1β1 heterodimer (17, 33) or the β1(1–194) construct did not produce an $O_2$-binding protein. Additionally, the I145Y mutation in the three sGC constructs led to different $Fe^{II}$-NO coordination states. Full-length α1β1 I145Y is mostly 6-coordinate (>85%) (17, 33) and β1(1–385) I145Y is mostly 5-coordinate (>90%) at 25 °C, but both are mixtures of 5- and 6-coordinate complexes. However, β1(1–194) I145Y exclusively formed a 5-coordinate complex (Figure S1), suggesting that the tyrosine is positioned differently in this protein compared to the full-length protein. Perhaps the distance from the distal pocket tyrosine to the bound ligand varies such that it is unable to form a hydrogen bond in the H-NOX protein. Alternatively, the PAS and CC domains may be involved in preventing the breaking of the Fe-His bond in the full-length protein.

### Kinetic characterization of β1 P118A and β1 I145Y mutants

In addition to influencing ligand coordination states, distal and proximal heme pocket modifications are known to influence ligand- binding kinetics. Heme oxidation in the presence of $O_2$ and NO dissociation from the heme were examined in the β1 mutants. It was previously determined that the β1 C-terminal truncation β1(1–194) produces a protein that is more susceptible to oxidation than the full-length protein (6). In this report the β1(1–385) oxidation rate was 4-fold slower than β1(1–194) and the full-length protein has no observable oxidation rate under the experimental conditions (Table 5). This demonstrates that the other domains on the β1 subunit and possibly the α1 subunit contribute to the remarkable stability of the $Fe^{II}$ heme state of the α1β1 heterodimer.

The effect of mutation within the proximal and distal heme pocket on $O_2$ binding and oxidation was further examined. Whereas the oxidation of β1(1–194) and β1(1–385) significantly increased (≥100-fold) in the P118A constructs, the α1β1 P118A heme did not oxidize even after 4 hrs at 37 °C in the presence of $O_2$ (Table 5). Additionally, no transient $Fe^{II}$-$O_2$ complex was observed during the oxidation of either β1(1–194) P118A or β1(1–385) P118A. The effect of this mutation on the β1 H-NOX truncations interaction with $O_2$ is more consistent with *Tt* H-NOX than α1β1. The dissociation of $O_2$ from *Tt* H-NOX decreased ~6-fold upon mutation of the corresponding proline to alanine (12). Since the $O_2$ association rate was unaffected by this mutation the net effect produced a protein with an increased affinity for $O_2$. While an observed $O_2$ off-rate can not be measured in the β1 constructs, it is clear that unlike in full-length sGC, mutation of Pro118 in β1(1–194) and β1(1–385) appreciably altered the affinity of the protein for $O_2$ and/or lowered the heme reduction potential.

In contrast to the dramatic effect on the H-NOX oxidation rate in the Pro118 mutant, the β1 I145Y mutation only slightly increased (≤2-fold) the oxidation rate of β1(1–194) and did not affect the oxidation rate of β1(1–385) (Table 5). In agreement with previous reports, no heme oxidation was observed in the full-length α1β1 I145Y protein (17, 33). Thus, the $Fe^{II}$ heme center is significantly influenced by the conformation of the full-length heterodimer. Perhaps the α1 subunit prevents $O_2$ from reaching the heme cofactor or influences the iron redox potential.

Since β1(1–385) I145Y is known to bind $O_2$ and mutation of proline 118 was shown to alter $O_2$ reactivity, the β1(1–385) P118A/I145Y double mutant was made to test if the mutations could synergistically alter the affinity for $O_2$. β1(1–385) P118A/I145Y purified with a substoichiometric amount of heme and was reconstituted as described. The reconstituted protein formed a 5-coordinate complex with NO and 6-coordinate complexes with both CO and $O_2$ (Table 4). Interestingly, the oxidation rate and observed $O_2$ association rate increased (3- and 5-fold, respectively) in the double mutant when compared to the I145Y mutant (Table 5). The presence of a tyrosine in the heme distal pocket significantly reduced the oxidation rate of β1(1–385) P118A (Figure 5), perhaps by stabilizing $O_2$ binding at the heme.

To further examine these sGC heme pocket mutants, the observed NO dissociation rate was measured using the CO/dithionite trapping method (14). Table S1 shows that despite significant changes in the susceptibility of the protein to $O_2$-induced oxidation, the NO dissociation rate in β1(1–194) P118A was not very different from the wild-type rate. NO dissociation from the β1 I145Y mutants was also examined (Figure S3). Previous reports have shown that the dissociation rate significantly increased in α1β1 I145Y (33); however, there were only slight changes in both the β1(1–194) I145Y and the β1(1–385) I145Y NO dissociation rates (< 2.5-fold). Clearly the most significant effect of the I145Y mutation was in the NO coordination state and NO dissociation rate of the full-length protein, and this

work shows that the heme domain truncations β1(1–194) and β1(1–385) do not mimic these effects. The varying properties of these mutants in the H-NOX constructs when compared to the α1β1 heterodimer suggest that the full-length protein has additional means to regulate ligand binding and heme reactivity. This regulation may involve a forced structural change in the heme pocket, which could alter potential hydrogen bonding contacts in the mutants.

### Probing the β1 heme environment with resonance Raman spectroscopy

It is known that mutation of the proximal pocket proline influences the heme conformation and Fe-His bond strength of *Tt* H-NOX (13). Specifically, several out-of-plane low frequency modes known to be sensitive to ruffling and saddling deformations exhibited a reduction in intensity and the Fe-His stretching frequency upshifted by 6 $cm^{-1}$ (13). The resonance Raman spectra of wild-type, P118A, and I145Y mutants of β1(1–194) in the $Fe^{II}$-unligated state were collected (Figure S4). Unfortunately this data could not be compared to the resonance Raman spectra of mutants in full-length sGC due to a high fluorescence background in these samples. In β1(1–194) P118A a slight upshift (2 $cm^{-1}$) in the $\nu_{Fe\text{-}His}$ band was observed (35) whereas, here, a slight downshift (3 $cm^{-1}$) is seen in β1(1–194) I145Y when compared to the wild-type protein. Therefore, the Fe-His bond strength decreases after mutation of Ile145 and increases after mutation of Pro118 (analogous to *Tt* H-NOX). In agreement with a previous report, there is no evidence for changes in heme conformation in these mutants based on the relative signal intensities of the low-frequency bands (35).

The RR $Fe^{II}$-CO spectra of the β1(1–385) and β1(1–194) I145Y mutants were also collected (Figure 6). In β1(1–194) I145Y there is a shift in the $\nu_{CO}$ band from 1969 to 1949 $cm^{-1}$ and in β1(1–385) I145Y there is a shift in the wild-type 492 $cm^{-1}$ $\nu_{FeC}$ band to 498 $cm^{-1}$. These shifts are likely due to a positive polar interaction between the introduced tyrosine and the bound CO (36). This interaction may affect the polarity around the ligand, weaken the heme propionate contacts with β1, and/or change the Fe-C-O angle (35).

The binding of NO and $O_2$ is significantly influenced by the PAS, CC and catalytic domains based on electronic absorption spectroscopy and kinetic analysis of site-directed mutants. These domains decrease the heme oxidation rate, perhaps by a mechanism that modulates $O_2$ accessibility and/or the iron redox potential. Allosteric interactions from these domains induce structural changes in the heme-binding pocket as evidenced by variations in the heme coordination state upon NO binding. Mutational analysis of conserved heme pocket residues also highlights the importance of studying the full-length protein to confirm biochemical predictions based on sGC truncations as some residues, like P118, significantly influence the ligand binding properties of isolated H-NOX proteins but not full-length sGC.

In summary, the β1 PAS, CC and catalytic domains can influence the heme environment of *Vc* H-NOX highlighting the structural similarity between sGC and non $O_2$-binding bacterial sGC homologs. Additionally, it was determined that Gcy-33 binds oxygen, in addition to NO and CO, and that the α1/Gcy33_β1 chimera is responsive to varying heme ligation states (Figure 7A). This suggests that atypical guanylate cyclases and NO sensitive guanylate cyclases have a common mechanism of domain regulation. While the precise molecular mechanism of this regulation remains to be determined, mutational analysis indicates that the allosteric interaction of the β1 PAS, CC and catalytic domains on the α1 and β1 subunits affects $O_2$ reactivity and NO dissociation (Figure 7B) - properties which are known to be essential to the physiological function of sGC in mammalian cells.

## Supplementary Material

Refer to Web version on PubMed Central for supplementary material.

## Acknowledgments

We thank Rosalie Tran and Richard Mathies for preliminary RR characterization of the $Fe^{II}$-unligated β1(1–194) constructs, Bryan Dickinson for preliminary purification of β1(1–194) mutants, Eric Underbakke for generating a graphic illustration of our sGC model, and Jonathan Winger for critical input on chimera design.

## Abbreviations

| | |
|---|---|
| **sGC** | soluble guanylate cyclase |
| **NO** | nitric oxide |
| **H-NOX** | Heme-Nitric oxide and OXygen binding domain |
| **PAS** | Per/ARNT/Sim |
| **RR** | resonance Raman |
| **YC-1** | 3-(5′-hydroxymethyl-3′-furyl)-1-benzylindazole |
| **DEA/NO** | diethylammonium (Z)-1-(N,N-diethylamino)diazen-1-ium-1,2- diolate |
| **DTT** | dithiothreitol |
| **Sf9** | *Spodoptera frugiperda* |
| **Hepes** | 4-(2-hydroxyethyl)-1-piperazineethane sulfonic acid |
| **DMSO** | dimethyl sulfoxide |
| **EIA** | enzyme immunoassay |

## References

1. Kemp-Harper B, Schmidt HH. cGMP in the vasculature. Handb Exp Pharmacol. 2009:447–467. [PubMed: 19089340]
2. Kleppisch T, Feil R. cGMP signalling in the mammalian brain: role in synaptic plasticity and behaviour. Handb Exp Pharmacol. 2009:549–579. [PubMed: 19089345]
3. Tsai EJ, Kass DA. Cyclic GMP signaling in cardiovascular pathophysiology and therapeutics. Pharmacol Ther. 2009; 122:216–238. [PubMed: 19306895]
4. Walter U, Gambaryan S. cGMP and cGMP-dependent protein kinase in platelets and blood cells. Handb Exp Pharmacol. 2009:533–548. [PubMed: 19089344]
5. Cary SP, Winger JA, Derbyshire ER, Marletta MA. Nitric oxide signaling: no longer simply on or off. Trends Biochem Sci. 2006; 31:231–239. [PubMed: 16530415]
6. Karow DS, Pan D, Davis JH, Behrends S, Mathies RA, Marletta MA. Characterization of functional heme domains from soluble guanylate cyclase. Biochemistry. 2005; 44:16266–16274. [PubMed: 16331987]
7. Zhao Y, Marletta MA. Localization of the heme binding region in soluble guanylate cyclase. Biochemistry. 1997; 36:15959–15964. [PubMed: 9398330]
8. Erbil WK, Price MS, Wemmer DE, Marletta MA. A structural basis for H-NOX signaling in Shewanella oneidensis by trapping a histidine kinase inhibitory conformation. P Natl Acad Sci USA. 2009; 106:19753–19760.
9. Ma X, Sayed N, Beuve A, van den Akker F. NO and CO differentially activate soluble guanylyl cyclase via a heme pivot-bend mechanism. Embo J. 2007; 26:578–588. [PubMed: 17215864]
10. Nioche P, Berka V, Vipond J, Minton N, Tsai AL, Raman CS. Femtomolar sensitivity of a NO sensor from Clostridium botulinum. Science. 2004; 306:1550–1553. [PubMed: 15472039]
11. Pellicena P, Karow DS, Boon EM, Marletta MA, Kuriyan J. Crystal structure of an oxygen-binding heme domain related to soluble guanylate cyclases. P Natl Acad Sci USA. 2004; 101:12854–12859.

12. Olea C, Boon EM, Pellicena P, Kuriyan J, Marletta MA. Probing the function of heme distortion in the H-NOX family. ACS Chem Biol. 2008; 3:703–710. [PubMed: 19032091]
13. Tran R, Boon EM, Marletta MA, Mathies RA. Resonance Raman spectra of an O2-binding H-NOX domain reveal heme relaxation upon mutation. Biochemistry. 2009; 48:8568–8577. [PubMed: 19653642]
14. Winger JA, Derbyshire ER, Marletta MA. Dissociation of nitric oxide from soluble guanylate cyclase and H-NOX domain constructs. J Biol Chem. 2007; 282:897–907. [PubMed: 17098738]
15. Winger JA, Derbyshire ER, Marletta MA. Dissociation of nitric oxide from soluble guanylate cyclase and H-NOX domain constructs. J Biol Chem. 2006; 282:897–907. [PubMed: 17098738]
16. Derbyshire ER, Marletta MA. Butyl isocyanide as a probe of the activation mechanism of soluble guanylate cyclase. Investigating the role of non-heme nitric oxide. J Biol Chem. 2007; 282:35741–35748. [PubMed: 17916555]
17. Derbyshire ER, Deng S, Marletta MA. Incorporation of tyrosine and glutamine residues into the soluble guanylate cyclase heme distal pocket alters NO and O2 binding. J Biol Chem. 2010; 285:17471–17478. [PubMed: 20231286]
18. Derbyshire ER, Marletta MA. Biochemistry of soluble guanylate cyclase. Handb Exp Pharmacol. 2009:17–31. [PubMed: 19089323]
19. Morton DB. Invertebrates yield a plethora of atypical guanylyl cyclases. Mol Neurobiol. 2004; 29:97–116. [PubMed: 15126679]
20. Zimmer M, Gray JM, Pokala N, Chang AJ, Karow DS, Marletta MA, Hudson ML, Morton DB, Chronis N, Bargmann CI. Neurons detect increases and decreases in oxygen levels using distinct guanylate cyclases. Neuron. 2009; 61:865–879. [PubMed: 19323996]
21. Boon EM, Marletta MA. Ligand specificity of H-NOX domains: from sGC to bacterial NO sensors. J Inorg Biochem. 2005; 99:892–902. [PubMed: 15811506]
22. Antonini, E.; Brunori, M. Hemoglobin and myoglobin in their reactions with ligands. North-Holland Pub. Co; Amsterdam: 1971.
23. Karow DS, Pan D, Tran R, Pellicena P, Presley A, Mathies RA, Marletta MA. Spectroscopic characterization of the soluble guanylate cyclase-like heme domains from Vibrio cholerae and Thermoanaerobacter tengcongensis. Biochemistry. 2004; 43:10203–10211. [PubMed: 15287748]
24. Huang SH, Rio DC, Marletta MA. Ligand binding and inhibition of an oxygen-sensitive soluble guanylate cyclase, Gyc-88E, from Drosophila. Biochemistry. 2007; 46:15115–15122. [PubMed: 18044974]
25. Ko FN, Wu CC, Kuo SC, Lee FY, Teng CM. YC-1, a novel activator of platelet guanylate cyclase. Blood. 1994; 84:4226–4233. [PubMed: 7527671]
26. Deinum G, Stone JR, Babcock GT, Marletta MA. Binding of nitric oxide and carbon monoxide to soluble guanylate cyclase as observed with resonance Raman spectroscopy. Biochemistry. 1996; 35:1540–1547. [PubMed: 8634285]
27. Derbyshire ER, Fernhoff NB, Deng S, Marletta MA. Nucleotide regulation of soluble guanylate cyclase substrate specificity. Biochemistry. 2009; 48:7519–7524. [PubMed: 19527054]
28. Hu X, Murata LB, Weichsel A, Brailey JL, Roberts SA, Nighorn A, Montfort WR. Allostery in recombinant soluble guanylyl cyclase from Manduca sexta. J Biol Chem. 2008; 283:20968–20977. [PubMed: 18515359]
29. Stasch JP, Becker EM, Alonso-Alija C, Apeler H, Dembowsky K, Feurer A, Gerzer R, Minuth T, Perzborn E, Pleiss U, Schroder H, Schroeder W, Stahl E, Steinke W, Straub A, Schramm M. NO-independent regulatory site on soluble guanylate cyclase. Nature. 2001; 410:212–215. [PubMed: 11242081]
30. Li ZQ, Pal B, Takenaka S, Tsuyama S, Kitagawa T. Resonance Raman evidence for the presence of two heme pocket conformations with varied activities in CO-bound bovine soluble guanylate cyclase and their conversion. Biochemistry. 2005; 44:939–946. [PubMed: 15654750]
31. Martin E, Czarnecki K, Jayaraman V, Murad F, Kincaid J. Resonance Raman and infrared spectroscopic studies of high-output forms of human soluble guanylyl cyclase. J Am Chem Soc. 2005; 127:4625–4631. [PubMed: 15796527]
32. Boon EM, Huang SH, Marletta MA. A molecular basis for NO selectivity in soluble guanylate cyclase. Nat Chem Biol. 2005; 1:53–59. [PubMed: 16407994]

33. Martin E, Berka V, Bogatenkova E, Murad F, Tsai AL. Ligand selectivity of soluble guanylyl cyclase: effect of the hydrogen-bonding tyrosine in the distal heme pocket on binding of oxygen, nitric oxide, and carbon monoxide. J Biol Chem. 2006; 281:27836–27845. [PubMed: 16864588]

34. Rothkegel C, Schmidt PM, Stoll F, Schroder H, Schmidt HHHW, Stasch JP. Identification of residues crucially involved in soluble guanylate cyclase activation. Febs Lett. 2006; 580:4205–4213. [PubMed: 16831427]

35. Ibrahim M, Derbyshire ER, Marletta MA, Spiro TG. Probing soluble guanylate cyclase activation by CO and YC-1 using resonance Raman spectroscopy. Biochemistry. 2010; 49:3815–3823. [PubMed: 20353168]

36. Spiro, TG.; Ibrahim, M.; Wasbotten, IH. CO, NO and $O_2$ as vibrational probes of heme protein active sites. In: Ghosh, A., editor. The smallest biomolecules: Diatomics and their interactions with heme proteins. Elsevier; Amesterdam: 2008. p. 96-123.

37. Denninger JW, Marletta MA. Guanylate cyclase and the NO/cGMP signaling pathway. Bba-Bioenergetics. 1999; 1411:334–350. [PubMed: 10320667]

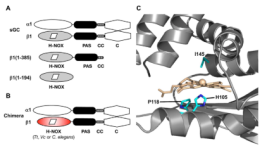

**Figure 1.**

Domain architecture of sGC α1β1, β1(1–385) and β1(1–194). H-NOX, PAS, coiled- coil (CC) and catalytic (C) domains are shown (**A**). Chimeras contain the *T. tengcongensis*, *V. cholerae* or *C. elegans* H-NOX domain fused to the rat β1 PAS, CC and C domains (**B**). Homology model of the rat β1 H-NOX domain (1U55.pdb) (**C**). Residues in the proximal pocket (His105 and Pro118) and in the distal pocket (Ile145) are shown.

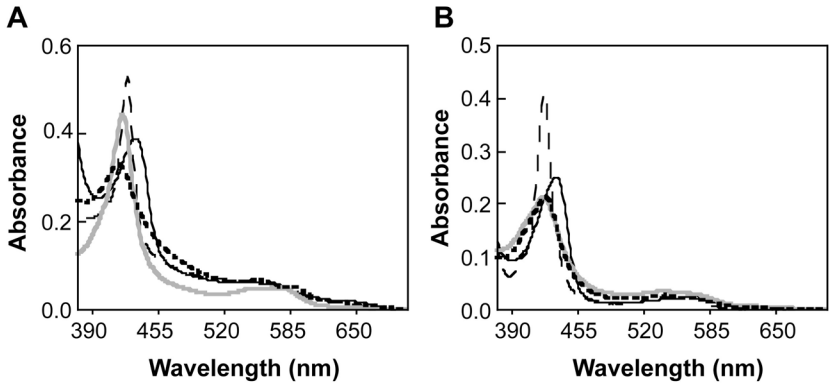


**Figure 2.**

Spectroscopic characterization of sGC chimeras. Electronic absorption spectra of α1/*Tt*_β1 (**A**) and α1/Gcy33_β1 (**B**) at 20 °C. $Fe^{II}$-unligated (black solid line), $Fe^{II}$-CO (black dashed line), $Fe^{II}$-NO (gray solid line) and $Fe^{II}$-$O_2$ (black dotted line) complexes are shown.

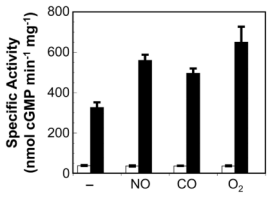


**Figure 3.**

Activity of sGC chimeras. Activity of α1/*Tt*_β1 (white bars) and α1/Gcy33_β1 (black bars) in the presence and absence of NO, CO, and $O_2$ at 37 °C. Samples of $Fe^{II}$-unligated protein contained 100 μM sodium dithionite.

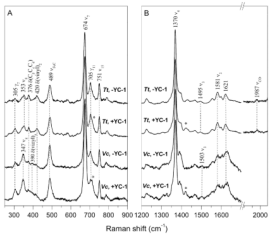


**Figure 4.**

Resonance Raman spectra of the α1/*Tt*_β1 and α1/*Vc*_β1 chimeric heterodimers in the $Fe^{II}$-CO state. Low- (*left panel*) and high- (*right panel*) frequency regions are shown for constructs in the absence and presence of YC-1 as indicated. The asterisk denotes bands from DMSO. The $\nu_{Fe\text{-}CO}$ and $\nu_{CO}$ stretching modes are indicated in the low- and high-frequency regions, respectively.

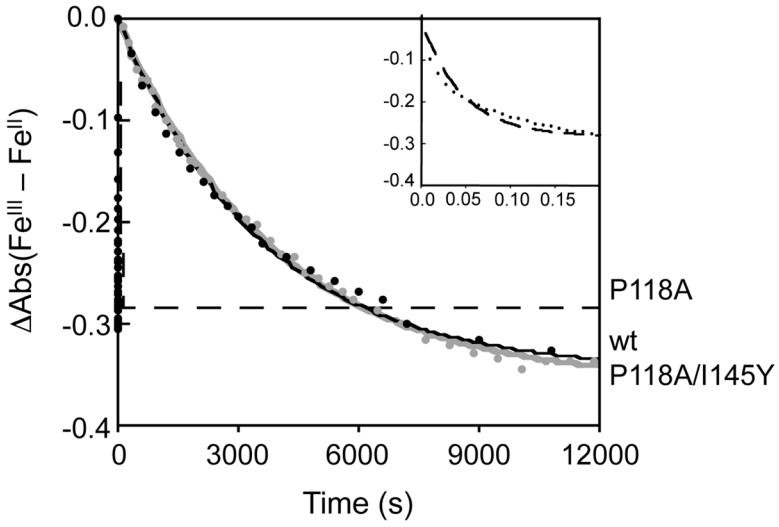


**Figure 5.**

Effect of heme pocket mutation on β1(1–385) oxidation rates. The change in absorbance of the $Fe^{III}$ Soret maximum minus the absorbance of the $Fe^{II}$ Soret maximum was plotted versus time. Data were fit with a single exponential. Time courses for wt (black solid line), P118A (black dashed line) and P118A/I145Y (gray solid line) are shown for β1(1–385). Inset shows the data for β1(1–385) P118A collected from 0 to 0.2 seconds.

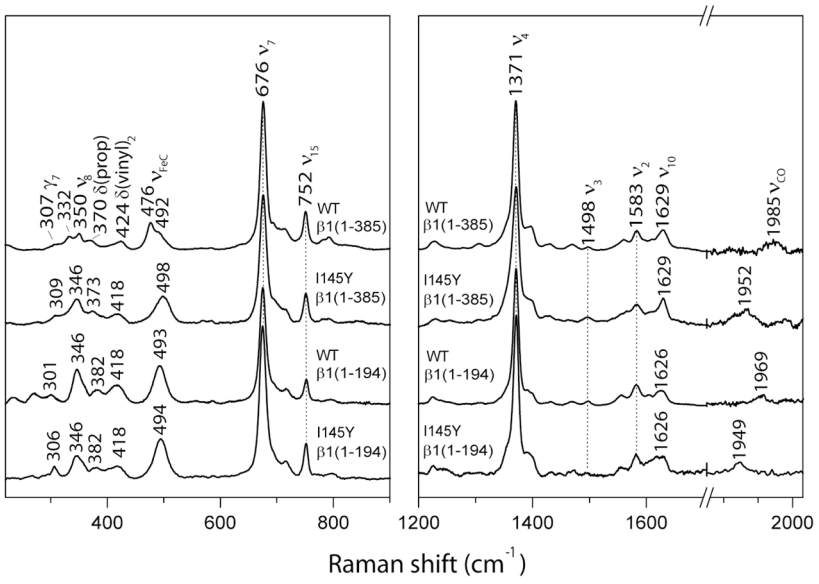


**Figure 6.**

Resonance Raman spectra of wt and I145Y β1(1–385) and β1(1–194) in the $Fe^{II}$-CO state. Low- (*left panel*) and high- (*right panel*) frequency regions are shown. The $\nu_{Fe\text{-}CO}$ and $\nu_{CO}$ stretching modes are indicated in the low- and high-frequency regions, respectively.

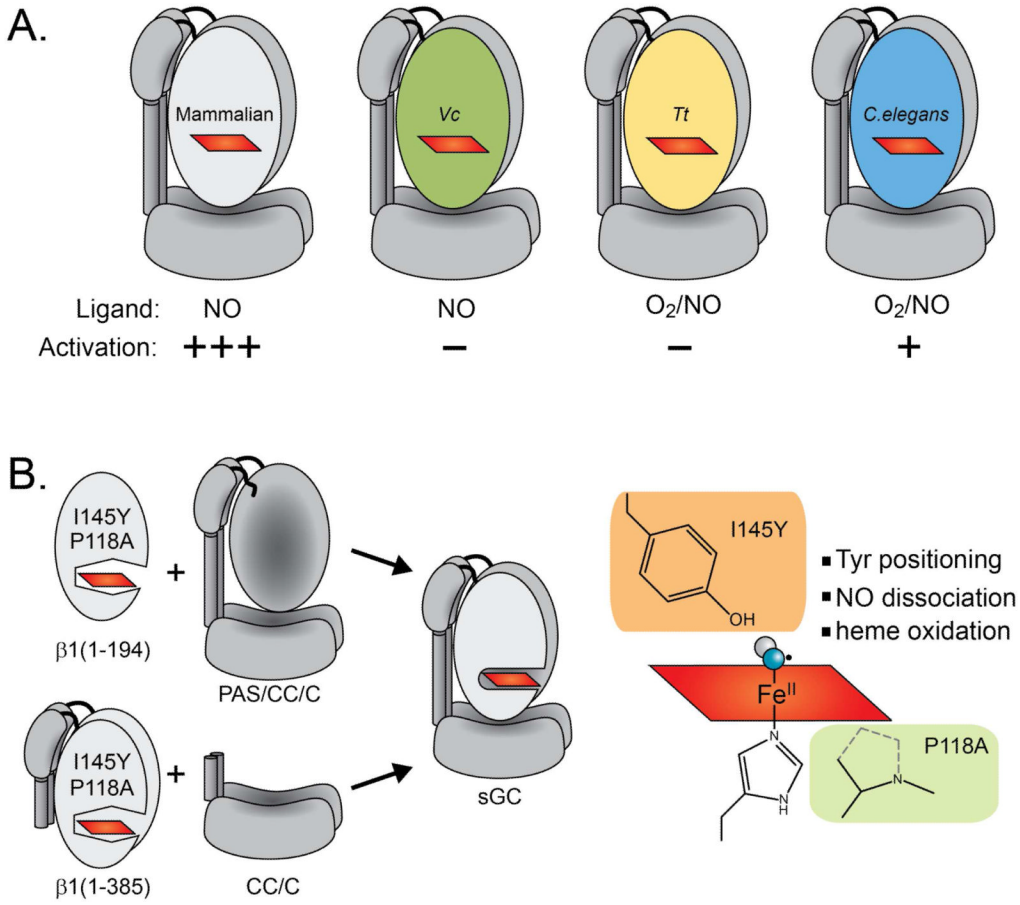


**Figure 7.**

Model of inter-domain communication. Fusion of *Vc* or *Tt* H-NOX domains to sGC produces a protein that does not respond to ligand binding at the heme, but fusion of the *C. elegans* Gcy-33 H-NOX domain influences the H-NOX heme environment and enzyme sensitivity to gaseous ligands (**A**). Mutation within the heme-binding pocket is influenced by the β1 PAS, CC and C domains on the α1 and β1 subunits (**B**). These observations indicate that allosteric interactions regulate sGC heme binding properties and enzyme activation.

## Table 1

Electronic absorption peak positions for sGC chimeras at 25 °C

| Protein | Ligand | Coor | Soret (nm) |
|---|---|---|---|
| α1/β1 | As isolated | 5 | 431 |
| | $Fe^{II}$-unligated | 5 | 431 |
| | $Fe^{II}$-NO | 5 | 399 |
| | $Fe^{II}$-CO | 6 | 423 |
| α1/$T_{t}$_ β1 | As isolated | 6 | 418–420 |
| | $Fe^{II}$-unligated | 5 | 432 |
| | $Fe^{II}$-NO | 6 | 420 |
| | $Fe^{II}$-CO | 6 | 423 |
| | $Fe^{II}$-$O_2$ | 6 | 420 |
| α1/*Vc*_ β1[a] | As isolated | ND[b] | 402/420 |
| | $Fe^{II}$-unligated | 5 | 426 |
| | $Fe^{II}$-NO | 5 | 401 |
| | $Fe^{II}$-CO | 6 | 420 |
| α1/Gcy33_ β1 | As isolated | ND[b] | 424 |
| | $Fe^{II}$-unligated | 5 | 433 |
| | $Fe^{II}$-NO | 6 | 422 |
| | $Fe^{II}$-CO | 6 | 421 |
| | FeII-$O_2$ | 6 | 418 |

[a] a1*Vc*_ β1 reconstituted with heme.

[b] ND; not determined.

## Table 2

Activity of sGC chimeras in various ligation states at 25 °C

| Protein | $Fe^{II}$ complex | Specific Activity (nmol cGMP $min^{-1}$ $mg^{-1}$) | Fold Change ($Fe^{II}$-unligated/$Fe^{II}$-X) | Fold Change (+YC-1/-YC-1) |
|---|---|---|---|---|
| α1/ β1 | $Fe^{II}$-unligated[b] | 58 ± 21 | 1 | 5 |
| | $Fe^{II}$-NO | 6054 ± 2303 | 77 | 19 |
| | $Fe^{II}$-CO | 124 ± 20 | 2 | 31 |
| α1/*Tt*_ β1 | $Fe^{II}$-unligated | 38 ± 2 | 1 | 1 |
| | $Fe^{II}$-NO | 36 ± 3 | 1 | 1 |
| | $Fe^{II}$-CO | 37 ± 0.3 | 1 | 1 |
| | $Fe^{II}$ + $O_2$ | 37 ± 2 | 1 | 1 |
| α1/*Vc*_ β1[a] | $Fe^{II}$-unligated | 44 ± 1 | 1 | 1 |
| | $Fe^{II}$-NO | 55 ± 14 | 1 | 1 |
| α1/Gcy33_ β1 | $Fe^{II}$-unligated | 326 ± 25 | 1 | ND[c] |
| | $Fe^{II}$-NO | 560 ± 28 | 1.7 | ND |
| | $Fe^{II}$-CO | 495 ± 24 | 1.5 | ND |
| | $Fe^{II}$ + $O_2$ | 650 ± 76 | 2 | ND |

[a] a1/*Vc*_ β1 reconstituted with heme.

[b] $Fe^{II}$-unligated data in the presence of 100 μM sodium dithionite.

[c] ND; not determined.

**Table 3**

Resonance Raman frequencies and mode assignments for various heme proteins in the $Fe^{II}$-CO ligation state[a]

| Protein | $\nu_2$ | $\nu_3$ | $\nu_4$ | ν(Fe-CO) | ν(C-O) | Ref. |
|---|---|---|---|---|---|---|
| α1β1 | 1582 | 1496 | 1371 | 473/493 | 1968/1988 | (26) |
| *Tt* H-NOX | 1580 | 1494 | 1369 | 490 | 1989 | (23) |
| α1/*Tt*_β1 | 1581 | 1495 | 1370 | 489 | 1987 | * |
| *Vc* H-NOX | 1578 | 1492 | 1367 | 491 | 1985 | (23) |
| α1/*Vc*_β1 | 1582 | 1503 | 1370 | 489 | N.D.[b] | * |

[a] Vibratins in $cm^{-1}$;

[b] N.D., not determined;

* This work.

**Table 4**

Electronic absorption peak positions for various sGC β1 mutants in α1β1 and H-NOX domains at 25 °C[a]

| Protein | Mutation | $Fe^{II}$ | $Fe^{II}$-NO | $Fe^{II}$-CO | $Fe^{II}$-$O_2$ | Ref. |
|---|---|---|---|---|---|---|
| α1β1 | wt | 431 | 399 | 423 | - | (37) |
| | β1 P118A | 428 | 399 | 420 | - | * |
| | β1 I145Y | 429 | **416**/399 | 423 | - | (33) |
| β1(1–385) | wt | 431 | 399 | 423 | - | (7) |
| | β1 P118A | 424 | 398 | 420 | - | * |
| | β1 I145Y | 428 | **400**/417 | 422 | 417 | (32), this work |
| | β1 P118A/β1 I145Y | 425 | 399 | 420 | 417 | * |
| β1(1–194) | wt | 431 | 398 | 423 | - | (6) |
| | β1 P118A | 428 | 398 | 421 | - | * |
| | β1 I145Y | 428 | 400 | 420 | - | * |

[a] Peak positions in nm;

* This work. In bold is the most abundant species of a mixture.

## Table 5

Comparison of kinetic parameters for various sGC β1 mutants in α1β1 and H-NOX domains at 37 °C

| Protein | Mutation | obs $K_{on}$ $O_2$ ($\mu M^{-1}$ $s^{-1}$) | $K_{ox}$ ($s^{-1}$) |
|---|---|---|---|
| α1β1 | wt | N.O.[a] | N.O. |
| | β1 P118A | N.O. | N.O. |
| | β1 I145Y | N.O. | N.O. |
| β1(1–385) | wt | N.O. | 0.00029 ± 0.00002 |
| | β1 P118A | N.O. | 17.6 ± 0.3[b] |
| | β1 I145Y | ~0.00004[c] | 0.00020[c] |
| | β1 P118AI145Y | 0.00012 ± 0.00003 | 0.00062 ± 0.00025 |
| β1(1–194) | wt | N.O. | 0.00121[d] |
| | β1 P118A | N.O. | 0.1950 ± 0.006 |
| | β1 I145Y | N.O. | 0.0022 ± 0.0005 |

[a] N.O., not observed;

[b] Rate measured and reported at 10 °C;

[c] Rates from (32);

[d] Rates from (6).